

# HYBRID SPHERICAL DESIGNS

MARTIN EHLER

*Faculty of Mathematics, University of Vienna, Austria*

**ABSTRACT.** Spherical  $t$ -designs are finite point sets on the unit sphere that enable exact integration of polynomials of degree at most  $t$  via equal-weight quadrature. This concept has recently been extended to spherical  $t$ -design curves by the use of normalized path integrals. However, explicit examples of such curves are rare.

We construct new spherical  $t$ -design curves for small  $t$  based on the edges of a distinct subclass of convex polytopes. We then introduce hybrid  $t$ -designs that combine points and curves for exact polynomial integration of higher degree. Our constructions are based on the vertices and edges of dual pairs of convex polytopes and polynomial invariants of their symmetry group. A notable result is a hybrid  $t$ -design for  $t = 19$ .

## 1 Introduction

Integration on the unit sphere serves as a fundamental tool in mathematics, physics, and engineering for analyzing and modelling phenomena with spherical symmetry. An effective approach for such integration is the concept of spherical designs. These are sets of points on the sphere that enable exact integration of polynomials up to a specific degree by using equal-weight quadrature formulas. Quadrature formulas in general are widely studied in numerical analysis, approximation theory, and signal processing, and although equal weights are not always necessary, they do simplify the formulas and make them more convenient and easier to use for practitioners.

*Points:* Formally, for  $t \in \mathbb{N}$ , let  $\Pi_t$  denote the space of all polynomials of total degree at most  $t$  in  $d + 1$  variables, restricted to the sphere  $\mathbb{S}^d = \{x \in \mathbb{R}^{d+1} : \|x\| = 1\}$ . A spherical  $t$ -design is a finite set of points  $X \subseteq \mathbb{S}^d$  with cardinality  $|X|$ , such that the normalized surface integral on the sphere can be exactly determined using the equal-weight quadrature formula

$$\frac{1}{|X|} \sum_{x \in X} \pi(x) = \int_{\mathbb{S}^d} \pi, \quad \text{for all } \pi \in \Pi_t.$$

This concept dates back to work by McLaren in 1963 [35], although the term ‘spherical design’ was coined later by Delsarte, Goethals, and Seidel in the 1970s [14].

---

*E-mail address:* martin.ehler@univie.ac.at.

*Date:* Martin February 19, 2025.

*2010 Mathematics Subject Classification.* 05B30, 52B15, 52B11.

*Key words and phrases.* spherical designs, edge-transitive polytopes, curves, geodesic cycles.

Since then, spherical  $t$ -designs have inspired a rich body of research investigating their explicit construction through analytic, algebraic, and numerical methods [3, 5–7, 13, 26, 30, 39, 41, 52].

*Curves:* While spherical designs have been extensively studied in the discrete setting, their continuous counterparts, spherical design curves, have been introduced only recently in [16]. These closed curves define a continuous path on the sphere and achieve the same exact integration property via normalized path integrals, i.e., a continuous function  $\gamma : [0, L] \rightarrow \mathbb{S}^d$  with  $\gamma(0) = \gamma(L)$  is a  $t$ -design curve if

$$\frac{1}{\ell(\gamma)} \int_{\gamma} \pi = \int_{\mathbb{S}^d} \pi, \quad \text{for all } \pi \in \Pi_t,$$

where  $\ell(\gamma)$  denotes the arc-length of  $\gamma$ .

Although constructions of families of  $t$ -design curves are provided in [17, 31], explicit examples of  $t$ -design curves are rare, even for modest values of  $t$ . Some new  $t$ -design curves are shown in Figures 1, 2, and 3.

*Curves for mobile sampling:* The concept of spherical design curves in [16] is motivated by mobile sampling, which studies the reconstruction of a function from its values along a curve [22, 45, 46]. Unlike discrete point sampling, such as with spherical design points that require multiple sensors, mobile sampling utilizes a single sensor that moves along a curved trajectory. An illustrative case of mobile sampling on the sphere involves gathering environmental data along an airplane flight path or the trajectory of a satellite, with the objective of reconstructing global information over the entire globe  $\mathbb{S}^2$ .

From a practical perspective, it makes sense to combine both sampling approaches by using a mobile device alongside static sensors where available. However, point-based and curve-based methods have traditionally been studied separately, and their combined use has remained largely unexplored within sampling theory and designs.

*Hybrid designs:* We propose the new notion of hybrid designs, where we consider both at the same time, a curve  $\gamma : [0, L] \rightarrow \mathbb{S}^d$  and finitely many points  $X \subseteq \mathbb{S}^d$ . We call the pair  $(\gamma, X)$  a hybrid  $t$ -design if there is a balancing constant  $0 \leq \rho \leq 1$  such that

$$\frac{\rho}{|X|} \sum_{x \in X} \pi(x) + \frac{1-\rho}{\ell(\gamma)} \int_{\gamma} \pi = \int_{\mathbb{S}^d} \pi, \quad \text{for all } \pi \in \Pi_t.$$

The benefit of hybrid designs in comparison to a ‘pure’ curve is increase of strength. Given a  $t$ -design curve  $\gamma$ , we may add a set of points  $X$  to enhance the integration strength to  $\Pi_s$  for some  $s > t$ , see Figures 4, 5, and 6.

## Main contributions

In this work, we expand the catalog of spherical designs by constructing new  $t$ -design curves and hybrid designs. The key findings are summarized as follows:

- (A) We construct several new  $t$ -design curves, some are shown in Figures 1, 2, and 3. These closed curves are obtained by projecting the edges of distinct convex polytopes onto the sphere as spherical arcs, and those arcs form a curve on

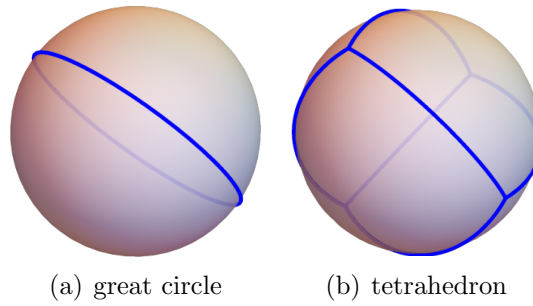


FIGURE 1. 1 and 2-designs.

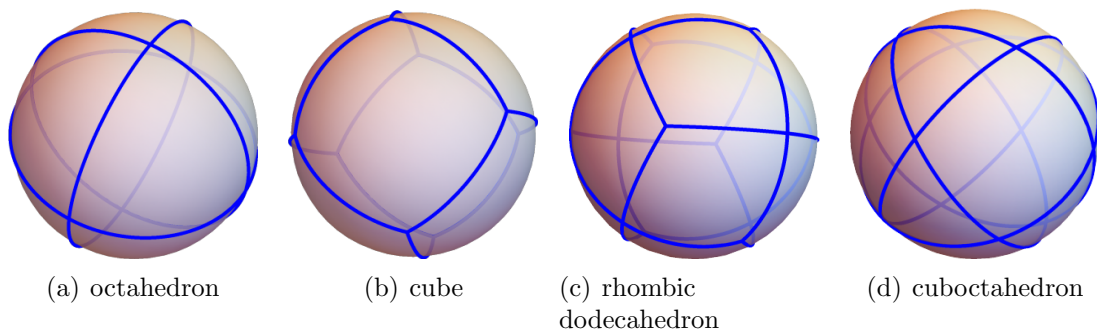


FIGURE 2. 3-designs.

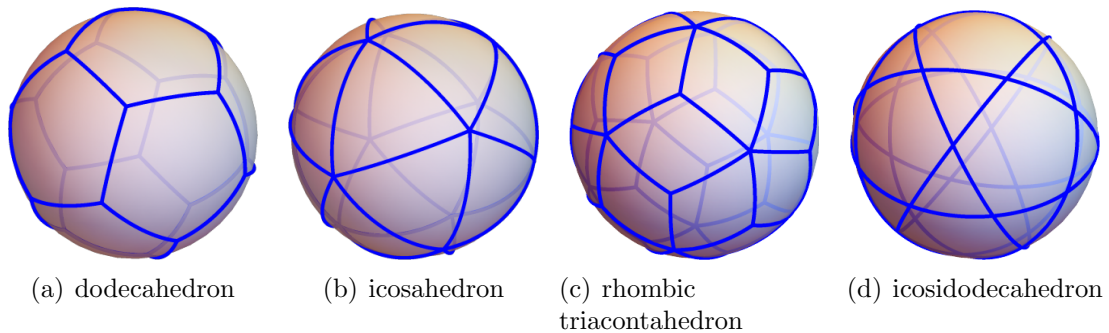


FIGURE 3. 5-designs.

the sphere. This construction relies on the symmetry properties of edge-transitive polytopes, whose symmetry group by definition acts transitively on the edges.

- (B) We derive the first hybrid  $t$ -designs, some are shown in Figures 4, 5, and 6. Our primary construction principle relies on distinct pairs of dual polytopes and their symmetry group, so that the curve  $\gamma$  is induced by the edges of the primal polytope projected onto the sphere and the points  $X$  are the vertices of the dual polytope. We use invariant theory [36] to determine the strength  $t$  of the hybrid design for several pairs of dual polytopes. This approach

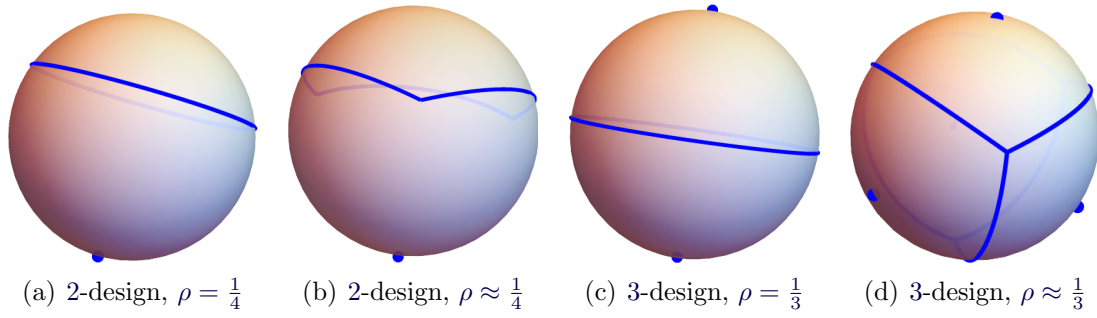


FIGURE 4. Hybrid 2- and 3-designs.

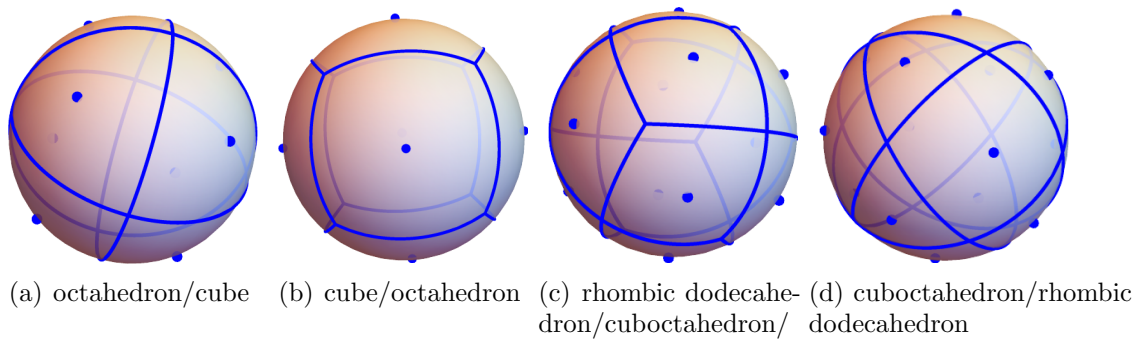


FIGURE 5. Hybrid 5-designs.

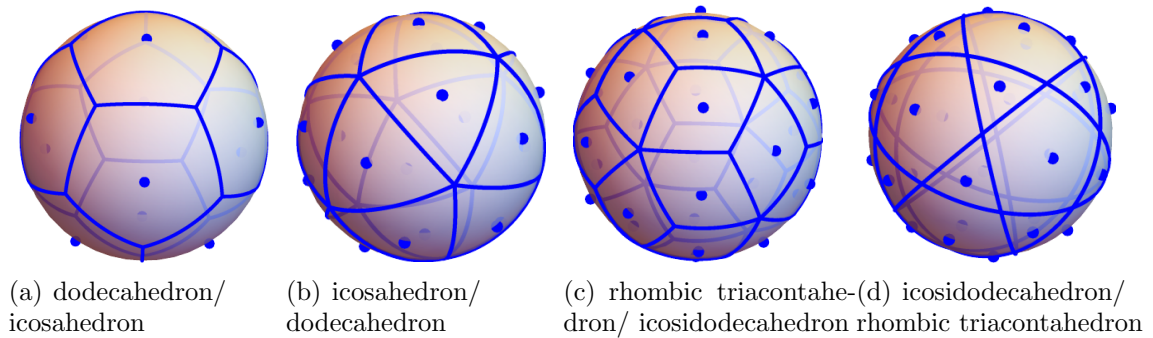


FIGURE 6. Hybrid 9-designs.

was guided by the ideas in [19, 35], where multiple orbits are used to derive weighted integration formulas.

- (C) As our strongest design, we obtain a hybrid 19-design on  $\mathbb{S}^3$  from group orbits that stands out from most of its competitors. To the best of our knowledge, the only competing construction is presented in [19], which provides spherical 19-design points. These two constructions produce the strongest spherical designs by analytic expressions, to our knowledge. In contrast, other spherical designs of similar or greater strength reported in the literature are typically obtained through numerical procedures, either on  $\mathbb{S}^2$  or  $\mathbb{S}^3$ , see [21, 24, 52] and

the associated websites<sup>1</sup>. These designs lack explicit analytic expressions and have not been rigorously proven to satisfy the conditions of a spherical 19-design. The existence results about asymptotically optimal spherical designs in [5, 6] are nonconstructive and hence do not provide any explicit designs.

*Outline:* In Section 2 we recall the concept of  $t$ -design curves, geodesic  $t$ -design cycles, and investigate the integration properties of group orbits of spherical arcs. New  $t$ -design curves are derived from convex polytopes in Section 3. The Sections 4 and 5 are dedicated to the new concept of hybrid  $t$ -designs and contain a construction principle from pairs of dual polytopes. We construct a hybrid 19-design in Section 6. In Section 7, we conclude the main part of our exposition by clarifying the fundamental idea of using invariants for exact integration, which becomes even more evident in the context of signed measures.

The appendix contains in Section A a table listing relevant properties of some edge-transitive polytopes. Section B contains the proof of Lemma 4.1 about the covering radius of spherical designs.

## 2 Curves, designs, and group orbits

We begin by introducing the concept of spherical  $t$ -design curves, as originally proposed in [16]. Next, we discuss integration along orbits of spherical arcs, which forms the foundation of our further investigations.

### 2.1 Spherical design curves

Here, a curve is defined as a continuous, piecewise smooth mapping  $\gamma : [0, L] \rightarrow \mathbb{S}^d$  that is closed in the sense that  $\gamma(0) = \gamma(L)$ . Given a continuous function  $\pi : \mathbb{S}^d \rightarrow \mathbb{R}$ , the path integral along  $\gamma$  is

$$\int_{\gamma} \pi = \int_0^L \pi(\gamma(\alpha)) \|\dot{\gamma}(\alpha)\| d\alpha,$$

and its arc-length is  $\ell(\gamma) = \int_{\gamma} 1$ . For  $t \in \mathbb{N}$ , recall that  $\Pi_t$  denotes the space of all polynomials of total degree at most  $t$  in  $d+1$  variables, restricted to the sphere. We follow [16] and call  $\gamma$  a spherical  $t$ -design curve if

$$\frac{1}{\ell(\gamma)} \int_{\gamma} \pi = \int_{\mathbb{S}^d} \pi, \quad \text{for all } \pi \in \Pi_t.$$

The parameter  $t$  is usually referred to as the strength of the design (curve). Unlike [16], we permit arbitrary self-intersections, so that the curve may traverse sections multiple times.

A piecewise smooth curve can be constructed by connecting finitely many points with geodesic arcs. To explicitly parametrize a geodesic arc, recall that the geodesic distance between points  $x$  and  $y$  on  $\mathbb{S}^d$  is given by

$$\text{dist}(x, y) = \arccos \langle x, y \rangle \in [0, \pi].$$

---

<sup>1</sup><https://www-user.tu-chemnitz.de/~potts/workgroup/graef/quadrature/index.php>  
<http://neilsloane.com/sphdesigns/>  
<https://web.maths.unsw.edu.au/~rsw/Sphere/EffSphDes/>

For  $y \neq \pm x$ , the distance is neither 0 nor  $\pi$ , and the geodesic arc is parametrized as  $\gamma_{x,y} : [0, \text{dist}(x, y)] \rightarrow \mathbb{S}^d$ ,

$$\gamma_{x,y}(s) = \frac{\sin(\text{dist}(x, y) - s)}{\sin(\text{dist}(x, y))} x + \frac{\sin(s)}{\sin(\text{dist}(x, y))} y.$$

Integration along a geodesic arc is direction-independent, so that  $\int_{\gamma_{x,y}} \pi = \int_{\gamma_{y,x}} \pi$ .

By connecting points  $x_1, \dots, x_n \in \mathbb{S}^d$  with such geodesic arcs, one obtains a geodesic chain, analogous to a polygonal chain in Euclidean space. For closed chains, called cycles, we set  $x_{n+1} := x_1$ . The integral over a cycle  $\gamma = (\gamma_{x_j, x_{j+1}})_{j=1}^n$  is

$$\int_{\gamma} \pi = \sum_{j=1}^n \int_{\gamma_{x_j, x_{j+1}}} \pi,$$

and the length of the cycle is the sum of the arc lengths  $\ell(\gamma) = \sum_{j=1}^n \text{dist}(x_j, x_{j+1})$ .

Every geodesic cycle  $\gamma$  induces a curve and is called a spherical  $t$ -design cycle (or  $t$ -design curve) if

$$\frac{1}{\ell(\gamma)} \int_{\gamma} \pi = \int_{\mathbb{S}^d} \pi \quad \text{for all } \pi \in \Pi_t.$$

In the following example we construct spherical  $t$ -design cycles derived from a set of great circles.

**Example 2.1** (Figures 2(a), 2(d), 3(d): arrangement of great circles in  $\mathbb{S}^2$ ). Consider a spherical  $t$ -design on  $\mathbb{S}^2$  of  $2n$  pairwise antipodal points [25]. Each line through antipodal points serves as the normal of a hyperplane, whose intersection with the sphere  $\mathbb{S}^2$  is a great circle. Hence, we end up with a set of  $n$  circles, which may serve as the trace of a curve.

To define this curve, we construct a graph whose vertices are the intersection points of these great circles, and whose edges are segments of the great circles connecting the vertices. An Euler cycle in this graph is a cycle that visits every edge exactly once. By Euler's Theorem on undirected, connected graphs, such a cycle exists if and only if each vertex has an even degree [47]. In our case, each vertex is attached to an even number of edges. Thus, the construction ensures the existence of an Euler cycle. This Euler cycle is a geodesic cycle on  $\mathbb{S}^2$ , and the results in [16] imply that it constitutes a  $t$ -design curve.

For instance, the 6 vertices of the octahedron and the 8 vertices of the cube each form a 3-design with pairwise antipodal points. The induced great circles lead to the trace of the edges of the spherical octahedron and the cuboctahedron as shown in Figures 2(a) and 2(d), respectively. The 12 vertices of the icosahedron are antipodal and form a 5-design. The associated 6 circles yield the trace of the spherical icosidodecahedron in Figure 3(d).

More explicit constructions of geodesic  $t$ -design cycles are provided in [17]. The present work focuses on constructions using group orbits.

## 2.2 Orbits of finite subgroups of the orthogonal group

A finite subgroup  $G$  of the orthogonal group  $\mathcal{O}(d+1)$  is called  $t$ -homogeneous in [4, 13] if every orbit  $X = \{gx_1 : g \in G\}$ , for  $x_1 \in \mathbb{S}^d$ , forms a spherical  $t$ -design. We



will make use of the finite Coxeter groups  $A_{d+1}$ ,  $B_{d+1}$ ,  $D_{d+1}$ , and the exceptional groups  $H_3$ ,  $F_4$ ,  $H_4$ ,  $E_6$ ,  $E_7$ , and  $E_8$  [28]. These are precisely the finite reflection groups in  $\mathcal{O}(d+1)$ , for  $d \geq 2$ , and the respective value of  $t$  is provided in [13], see also Table 1 and Table 3 in the appendix. A more detailed analysis of  $H_4$  and  $E_8$  in regard to spherical designs is contained in [37].

To expand exact integration from point orbits to orbits of geodesic arcs, we consider the space of  $G$ -invariant polynomials of degree at most  $t$  given by

$$\Pi_t^G := \{\pi \in \Pi_t : \pi \circ g = \pi \text{ for all } g \in G\}.$$

It is already observed in [13, 19] that the group  $G$  is  $t$ -homogeneous if and only if  $\Pi_t^G$  consists solely of constant functions. In other words,  $\Pi_t^G$  is one-dimensional, commonly denoted by  $\Pi_t^G = \mathbb{R}$ .

This formulation enables us to derive exact integration for orbits of geodesic arcs.

**Lemma 2.1.** *If  $G \subseteq \mathcal{O}(d+1)$  is  $t$ -homogeneous and  $\gamma_1 \subseteq \mathbb{S}^d$  is a geodesic arc, then the orbit  $(g\gamma_1)_{g \in G}$  induced by  $\gamma_1$  satisfies the exact integration condition*

$$\frac{1}{|G|} \sum_{g \in G} \frac{1}{\ell(\gamma_1)} \int_{g\gamma_1} \pi = \int_{\mathbb{S}^d} \pi, \quad \text{for all } \pi \in \Pi_t.$$

If  $\gamma_1$  is a constant curve, so that  $\gamma_1(s) = x_1 \in \mathbb{S}^d$ , for  $s \in [0, 1]$ , then the integration reduces to a point evaluation  $\frac{1}{\ell(\gamma_1)} \int_{g\gamma_1} \pi = \pi(gx_1)$ . Thus, each orbit  $Gx_1$  is a  $t$ -design, as mentioned above and used in [35].

*Proof.* For  $\pi \in \Pi_t$ , we denote its  $G$ -invariant average by

$$\pi^G := \frac{1}{|G|} \sum_{g \in G} \pi \circ g.$$

This average leads to the compact expression

$$\frac{1}{|G|} \sum_{g \in G} \frac{1}{\ell(\gamma_1)} \int_{g\gamma_1} \pi = \frac{1}{|G|} \sum_{g \in G} \frac{1}{\ell(\gamma_1)} \int_{\gamma_1} \pi \circ g = \frac{1}{\ell(\gamma_1)} \int_{\gamma_1} \pi^G.$$

Since  $G$  is  $t$ -homogeneous,  $\pi^G$  is constant and we trivially obtain

$$\frac{1}{\ell(\gamma_1)} \int_{\gamma_1} \pi^G = \int_{\mathbb{S}^d} \pi^G.$$

The orthogonal invariance of the measure on  $\mathbb{S}^d$  leads to  $\int_{\mathbb{S}^d} \pi \circ g = \int_{\mathbb{S}^d} \pi$ , for all  $g \in G$ , and hence  $\int_{\mathbb{S}^d} \pi^G = \int_{\mathbb{S}^d} \pi$ , which concludes the proof.  $\blacksquare$

Starting with an arbitrary spherical arc  $\gamma_1$ , the orbit of geodesic arcs  $\Gamma = \{g\gamma_1 : g \in G\}$  is generally not a connected set. As a result, it does not form a geodesic cycle. To overcome this issue, we will soon introduce additional structure to the orbit  $\Gamma$ . This structure is provided by convex polytopes, which are discussed next.

### 3 Spherical $t$ -design cycles from convex polytopes

A convex polytope  $\mathcal{P}$  in  $\mathbb{R}^d$  is defined as the convex hull of a finite set of points in  $\mathbb{R}^d$ . We assume  $\mathcal{P}$  is centered at the origin and scaled such that it lies within the unit ball. By projecting outward, each edge of the polytope defines a geodesic arc on the unit sphere.

To construct a geodesic cycle on the sphere, we use that the vertices and edges of the polytope define a graph. An Euler cycle traverses each edge of the graph exactly once, and according to Euler's theorem, a connected graph has an Euler cycle if every vertex is incident with an even number of edges, cf. Example 2.1. By outward projection, such an Euler cycle translates directly into a geodesic cycle on the sphere.

If not all vertices are incident to an even number of edges, we double all edges of the graph. This modified graph ensures that all vertices now meet the conditions for admitting an Euler cycle.

#### 3.1 Euler cycles of convex polytopes induce spherical $t$ -design cycles

The symmetries of a convex polytope  $\mathcal{P}$  in  $\mathbb{R}^d$  are the elements  $g \in \mathcal{O}(d)$  that leave  $\mathcal{P}$  invariant, i.e.,  $g\mathcal{P} = \mathcal{P}$ . These elements constitute the (full) symmetry group  $G$  of  $\mathcal{P}$ , which also acts on the geometric features of the polytope.

One such feature is a face and defined as the intersection of the polytope with a hyperplane, so that the polytope lies entirely on one side of the hyperplane. Faces can range from vertices (0-dimensional faces) and edges (1-dimensional faces) all the way up to facets ( $d - 1$ -dimensional faces) and the polytope itself ( $d$ -dimensional face).

A (proper) flag is a tuple  $f = (f_0, f_1, \dots, f_{d-1})$  of nested faces of the polytope, so that each  $f_k$  is  $k$ -dimensional, and  $f_{k-1} \subseteq f_k$  for  $k = 1, \dots, d-1$ . A convex polytope in  $\mathbb{R}^d$  is called regular if its symmetry group  $G$  acts transitively on its flags. That is, for any two flags  $f$  and  $f'$ , there exists  $g \in G$  such that  $f' = gf$ .

In particular, regular convex polytopes are  $k$ -face-transitive for all  $k = 0, \dots, d-1$ , i.e., their symmetry group acts transitively on their  $k$ -dimensional faces. Consequently, each set of  $k$ -dimensional faces forms a single orbit under the action of  $G$ .

If the symmetry group  $G$  of a convex polytope is  $t$ -homogeneous, vertex-transitivity (transitivity on 0-dimensional faces) ensures that the vertices, when projected onto the sphere, form a  $t$ -design. We now extend this observation from vertices to edges.

**Theorem 3.1.** *Suppose that  $\mathcal{P}$  is an edge-transitive convex polytope in  $\mathbb{R}^{d+1}$ . If its symmetry group  $G \subseteq \mathcal{O}(d+1)$  is  $t$ -homogeneous, then every Euler cycle projected onto the sphere  $\mathbb{S}^d$  is a spherical  $t$ -design cycle.*

If the assumptions of Theorem 3.1 are satisfied but  $\mathcal{P}$  does not admit any Euler cycles, then as mentioned before we may double each edge and every Euler cycle in this new configuration yields a geodesic  $t$ -design cycle.

*Proof.* Let  $(e_i)_{i=1}^m$  denote all edges of  $\mathcal{P}$  ordered according to an Euler cycle and let  $\gamma = (\gamma_i)_{i=1}^m$  be the induced geodesic cycle on the sphere, so that  $\gamma_i$  is the geodesic arc induced by projecting the edge  $e_i$  onto the sphere.



polytope	symmetry	$t$	# vertices	# edges
tetrahedron	$T_d = A_3$	2	4	6
octahedron	$O_h = B_3$	3	6	12
cube	$O_h = B_3$	3	8	12
icosahedron	$I_h = H_3$	5	12	30
dodecahedron	$I_h = H_3$	5	20	30
cuboctahedron	$O_h = B_3$	3	12	24
rhombic dodecahedron	$O_h = B_3$	3	14	24
icosidodecahedron	$I_h = H_3$	5	30	60
rhombic triacontahedron	$I_h = H_3$	5	32	60

TABLE 1. List of all edge-transitive convex polytopes in  $\mathbb{R}^3$ .

Since  $G$  acts transitively on the edges, the edges form a single orbit  $\{e_1, \dots, e_m\} = \{ge_1 : g \in G\}$ . For every  $g \in G$ , the edge  $ge_1$  corresponds to the geodesic arc  $g\gamma_1$ . Thus,  $G$  also acts transitively on the arcs. Since the cardinality of an orbit divides the group order, we deduce

$$\frac{1}{m} \sum_{i=1}^m \frac{1}{\ell(\gamma_i)} \int_{\gamma_i} \pi = \frac{1}{|G|} \sum_{g \in G} \frac{1}{\ell(\gamma_1)} \int_{g\gamma_1} \pi.$$

Lemma 2.1 implies the integration condition

$$\frac{1}{m} \sum_{i=1}^m \frac{1}{\ell(\gamma_i)} \int_{\gamma_i} \pi = \int_{S^d} \pi, \quad \text{for all } \pi \in \Pi_t,$$

so that the Euler cycle projected onto the sphere is a spherical  $t$ -design cycle.  $\blacksquare$

The class of edge-transitive polytopes has not yet been fully characterized [23, 32, 49], but several edge-transitive convex polytopes are known and subclasses have been studied [48].

### 3.2 Edge-transitive convex polytopes in $\mathbb{R}^3$

All edge-transitive convex polytopes in  $\mathbb{R}^3$  are known [20], and there are 9 of them, see Table 1. Five are the regular convex polytopes, namely the platonic solids. These are the tetrahedron, the octahedron, the cube, the icosahedron, and the dodecahedron. Their symmetries are the tetrahedral group  $T_d = A_3$ , the octahedral group  $O_h = B_3$ , and the icosahedral group  $I_h = H_3$ , that are  $t$ -homogeneous for  $t = 2, 3, 5$ , respectively. The indices d and h stand for 'dihedral' and 'holohedral', so that we refer to the full groups of cardinalities 24, 48, and 120, respectively. The other four edge-transitive convex polytopes are the cuboctahedron, the icosidodecahedron, the rhombic dodecahedron, and the rhombic triacontahedron.

Table 1 provides a summary of the relevant properties of those nine polytopes. The induced geodesic  $t$ -design cycles as claimed in Theorem 3.1 are shown in Figures 1, 2, and 3 in the introduction.

### 3.3 Further edge-transitive polytopes

We provide a list of some edge-transitive polytopes in  $\mathbb{R}^d$  in Table 3 in the appendix. All regular convex polytopes in  $\mathbb{R}^d$  are edge-transitive. Among these, three types exist in every dimension: the  $d$ -dimensional regular simplex (often referred to as the  $d$ -dimensional tetrahedron), the  $d$ -dimensional cube, and the  $d$ -dimensional octahedron.

The dimension  $d = 4$  is unique, as  $\mathbb{R}^4$  contains six convex regular polytopes. In addition to the 4-tetrahedron (5-cell), the 4-octahedron (16-cell), and the 4-cube (8-cell), there are the hypericosahedron (600-cell), the hyperdodecahedron (120-cell), and the 24-cell.

For a convex regular polytope  $\mathcal{P}$ , its rectified polytope  $\mathcal{P}_{\text{rect}}$  is defined as the convex hull of the midpoints of its edges, and they form another subclass of edge-transitive polytopes [49].

A notable further subclass of edge-transitive polytopes are the distance-transitive convex polytopes, as introduced in [48]. Examples include the  $2_{21}$ -polytope in  $\mathbb{R}^6$  and the  $3_{21}$ -polytope in  $\mathbb{R}^7$  [48, Theorem 5.10]. The  $2_{21}$ -polytope connects each vertex by 16 edges, allowing Euler cycles, while the  $3_{21}$ -polytope connects vertices with 27 edges, requiring edge doubling. Their symmetry groups,  $E_6$  and  $E_7$ , are 4- and 5-homogeneous [13] and enable the construction of spherical 4- and 5-design cycles, respectively. The  $d$ -demi-cube in  $\mathbb{R}^d$  is also distance-transitive and its symmetry group  $D_d$  is 3-homogeneous.

The  $4_{21}$ -polytope in  $\mathbb{R}^8$ , also known as the  $E_8$  root polytope, is edge-transitive [50, Proposition 4] but not distance-transitive [48, Theorem 5.10]. Its symmetry group,  $E_8$ , is 7-homogeneous [13]. Consequently, the family of  $k_{21}$ -polytopes in  $\mathbb{R}^{4+k}$  for  $k = 0, \dots, 4$  is edge-transitive. Here,  $0_{21}$  is the rectified 4-simplex, and  $1_{21}$  is the 5-demicube, both of which have been mentioned earlier in this section.

For a brief summary and few more details, we refer to Table 3 in the appendix.

## 4 Hybrid spherical designs

The  $t$ -design curves discussed in the previous sections are based on edge-transitive polytopes. This approach utilizes their  $t$ -homogeneous symmetry groups and produces several new  $t$ -design curves. However, the achievable range of the degree  $t$  is limited. The highest value of  $t$  in Table 3 is 11 and corresponds to the symmetry group  $H_4$  of the 120-cell and 600-cell. The examples in  $\mathbb{R}^3$  are restricted to the degrees  $t = 2, 3, 5$ .

To achieve higher degrees, we introduce the concept of hybrid designs that combine a spherical (design) curve with additional (design) points.

### 4.1 Introduction to hybrid designs

In sampling theory, the path of a curve can model a mobile sensor, while individual points correspond to static sensors. To improve coverage and integration capabilities, we now combine curves and points. In particular, we may balance the contributions of static and mobile sensors by an additional factor  $\rho$ .

**Definition 4.1** (hybrid  $t$ -designs). Given a curve  $\gamma$  on  $\mathbb{S}^d$  and a finite set  $X \subseteq \mathbb{S}^d$ , we call the pair  $(\gamma, X)$  a hybrid  $t$ -design if there is a constant  $0 \leq \rho \leq 1$  such that

$$(1) \quad \frac{\rho}{|X|} \sum_{x \in X} \pi(x) + \frac{1-\rho}{\ell(\gamma)} \int_{\gamma} \pi = \int_{\mathbb{S}^d} \pi, \quad \text{for all } \pi \in \Pi_t.$$

Evaluation for  $\pi \equiv 1$  implies that the contributions of the points and the curve need to be balanced by an affine combination, which leads to the factors  $\rho$  and  $1 - \rho$  in (1). In the context of numerical quadrature, it is reasonable to require that both, the points and the curve, contribute positively. This leads to the condition  $0 < \rho < 1$ . If  $\gamma$  is a  $t$ -design curve and  $X \subseteq \mathbb{S}^d$  are  $t$ -design points, then  $(\gamma, X)$  is a hybrid  $t$ -design for every  $\rho$ . The artificial choice  $\rho = 0$  or  $\rho = 1$  is associated to pure designs that consist of either a curve or points exclusively. The balancing factor offers a degree of freedom not available in pure designs. If we do not want to specify  $t$ , we may simply say 'hybrid design'.

The integration formula can be interpreted as being induced by a probability measure on  $\mathbb{S}^d$  whose support consists of points and the trajectory of a curve. For general probability measures, we now derive a necessary covering property that provides insight into how the points should be positioned relative to the curve. The covering radius of a closed subset  $M \subseteq \mathbb{S}^d$  is defined as

$$\delta(M) := \sup_{x \in \mathbb{S}^d} \min_{y \in M} \text{dist}(x, y),$$

representing the radius of the largest open ball in  $\mathbb{S}^d$  that does not intersect  $M$ .

While explicit upper bounds on the covering radius of spherical design points, particularly for small  $t$ , are derived in [43], the following result illustrates that the curve and the points of a hybrid design must also cover the sphere sufficiently well.

**Lemma 4.1.** *There is a constant  $C_d > 0$ , depending on the dimension  $d$ , such that the following holds: If  $\mu$  is a probability measure on  $\mathbb{S}^d$  such that*

$$(2) \quad \int_{\mathbb{S}^d} \pi(x) d\mu(x) = \int_{\mathbb{S}^d} \pi, \quad \text{for all } \pi \in \Pi_t,$$

*then the covering radius of the support of  $\mu$  satisfies*

$$\delta(\text{supp}(\mu)) \leq C_d t^{-1}.$$

For probability measures with finite support, this result is contained in [38] and shows that the upper bounds in [43] do not have the optimal asymptotics for large  $t$ . The more general claim in Lemma 4.1 might also be well-known to the experts (see [33,34] for related results). For instance, it can be derived from the lines of the first part of the proof in [16, Theorem 2.2], and we provide the details in the Appendix B for the sake of completeness.

Since the constant  $C_d$  is not specified here, Lemma 4.1 does not offer a direct bound on the covering radius for specific hybrid  $t$ -designs. It rather suggests that a smaller covering radius is preferable, meaning points should be placed to fill gaps where the curve has large voids. We continue with a few elementary hybrid designs in Figures 4(a), 4(b), and 4(c) that illustrate this idea.

**Proposition 4.2.** *The following configurations form hybrid designs:*

- (i) *Figure 4(a): a circle parallel to the equator at height  $\frac{1}{3}$  paired with the south pole  $x_S = (0, 0, -1)^\top$  forms a hybrid 2-design with  $\rho = \frac{1}{4}$ .*
- (ii) *Figure 4(b): the south pole  $x_S$  and a regular spherical triangle centered around the north pole at the correct height form a hybrid 2-design.*
- (iii) *Figure 4(c): the equator paired with the north pole  $x_N = (0, 0, 1)^\top$  and the south pole  $x_S$  yield a hybrid 3-design with  $\rho = \frac{1}{3}$ .*

*Proof.* It is sufficient to check the integration conditions for the monomials. We used the computer algebra system Mathematica [51] to streamline the proof, but all symbolic calculations remain verifiable by hand.

The orthogonal invariance of the surface measure of  $\mathbb{S}^2$  yields that the integral  $\int_{\mathbb{S}^2} x^k y^l z^m$  vanishes if at least one of the exponents  $k, l, m \in \mathbb{N}$  is odd. Moreover, the identity  $x^2 + y^2 + z^2 = 1$  leads to  $\int_{\mathbb{S}^2} x^2 = \int_{\mathbb{S}^2} y^2 = \int_{\mathbb{S}^2} z^2 = \frac{1}{3}$ .

- (i) A circle at height  $0 \leq r \leq 1$  is parametrized by  $\gamma_r : [0, 1] \rightarrow \mathbb{S}^2$ ,

$$(3) \quad \gamma_r(\alpha) = (\cos(\alpha)\sqrt{1-r^2}, \sin(\alpha)\sqrt{1-r^2}, r)^\top.$$

We observe  $\int_{\gamma_r} x = \int_{\gamma_r} y = 0$  and the respective point evaluations at the south pole also vanish. We now let the balancing factor  $\rho(r)$  depend on  $r$ . Since  $\frac{1}{\ell(\gamma_r)} \int_{\gamma_r} z = r$ , to match  $\int_{\mathbb{S}^2} z = 0$ , we require  $-\rho(r) + (1 - \rho(r))r = 0$ . Thus,  $\rho(r) = \frac{r}{1+r}$  yields that  $(\gamma_r, \{x_S\})$  is a hybrid 1-design.

For  $r = \frac{1}{3}$ , we obtain  $\rho(r) = \frac{1}{4}$  and  $\frac{1}{\ell(\gamma_r)} \int_{\gamma_r} z^2 = \frac{1}{9}$ . The sum of the point evaluation and the path integral of the monomial  $z^2$  is  $\frac{1}{4} + (1 - \frac{1}{4})\frac{1}{9} = \frac{1}{3}$ , which matches  $\int_{\mathbb{S}^2} z^2 = \frac{1}{3}$ . The symmetry of the configuration and  $x^2 + y^2 + z^2 = 1$  eventually imply that the analogous evaluation for the monomials  $x^2$  and  $y^2$  also yields  $\frac{1}{3}$ , so that we obtain a hybrid 2-design.

(iii) If  $r = 0$  in (3), then the pair  $(\gamma_0, \{x_N, x_S\})$  is antipodal, and hence the exact integration identities are satisfied when the sum  $k+l+m$  is odd. It remains to check the monomials  $xy, xz, yz$ , and  $x^2, y^2, z^2$ . Direct calculations based on symmetries reveal that  $(\gamma_0, \{x_N, x_S\})$  ‘integrates’  $xy, xz, yz$  to zero. To match  $\int_{\mathbb{S}^2} z^2 = \frac{1}{3}$ , we may simply choose  $\rho = \frac{1}{3}$  since the equator does not contribute in that case. For the remaining cases  $x^2$  and  $y^2$ , the poles do not contribute and we obtain

$$\frac{2}{3} \frac{1}{\ell(\gamma_0)} \int_{\gamma_0} x^2 = \frac{2}{3} \frac{1}{\ell(\gamma_0)} \int_{\gamma_0} y^2 = \frac{1}{3}.$$

Thus,  $(\gamma_0, \{x_N, x_S\})$  is a hybrid 3-design.

(ii) This configuration is more elaborate. For  $a \in (0, \frac{\pi}{2}]$ , we parametrize the triangle around the north pole by the three control points

$$p_1 = \begin{pmatrix} \sin(a) \\ 0 \\ \cos(a) \end{pmatrix}, \quad p_2 = \begin{pmatrix} -\frac{1}{2} \sin(a) \\ \frac{\sqrt{3}}{2} \sin(a) \\ \cos(a) \end{pmatrix}, \quad p_3 = \begin{pmatrix} -\frac{1}{2} \sin(a) \\ -\frac{\sqrt{3}}{2} \sin(a) \\ \cos(a) \end{pmatrix}.$$

We now solve the resulting equations for the monomials in the parameter  $a$ . To match  $\int_{\mathbb{S}^2} z = 0$ , symbolic calculations yield

$$(4) \quad \rho(a) = \frac{1}{1 + \frac{\sqrt{5+3\cos(2a)}}{\sqrt{6}\sin(2a)} \arccos(\frac{1}{4} + \frac{3}{4}\cos(2a))} \in [0, \frac{1}{2}],$$

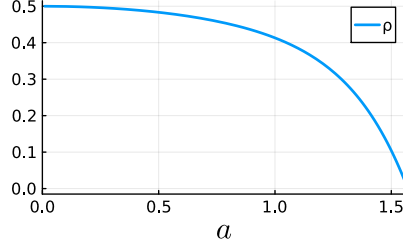


FIGURE 7. The factor  $\rho(a)$  in (4) balances the contribution of the south pole with the triangle at height  $\cos(a)$  in the proof of Part (ii) of Proposition 4.2. We obtain a hybrid 2-design at  $\hat{a} \approx 1.359$  with  $\rho(\hat{a}) \approx 0.249$ .

see Figure 7. This also matches  $\int_{\mathbb{S}^2} x = \int_{\mathbb{S}^2} y = 0$ , so that the south pole paired with the triangle forms a hybrid 1-design for the balancing factor  $\rho(a)$ .

To derive a hybrid 2-design, we must now select  $a$ . We denote the triangle by  $\gamma_a$ . For  $i = 1, 2, 3$ , define the continuous functions

$$U_i(a) := \rho(a)\pi_i(0, 0, -1) + \frac{1 - \rho(a)}{\ell(\gamma_a)} \int_{\gamma_a} \pi_i,$$

where  $\pi_1, \pi_2$ , and  $\pi_3$  are the monomials  $x^2, y^2$ , and  $z^2$ , respectively. Symmetry leads to the identity  $U_1(a) = U_2(a)$ , for all  $a \in (0, \frac{\pi}{2})$ . To identify  $\hat{a} \in (0, \frac{\pi}{2})$  such that  $U_1(\hat{a}) = U_3(\hat{a})$ , we prepare to apply the mean value theorem.

For  $a = \frac{\pi}{2}$ , the spherical triangle  $\gamma_a$  coincides with the equator, and  $a \approx 0$  deforms the triangle  $\gamma_a$  into the north pole. We observe  $\rho(0) = \frac{1}{2}$  and  $\rho(\frac{\pi}{2}) = 0$ , so that

$$\begin{aligned} \lim_{a \searrow 0} U_1(a) &= 0, & U_1(\frac{\pi}{2}) &> 0, \\ \lim_{a \searrow 0} U_3(a) &= 1, & U_3(\frac{\pi}{2}) &= 0, \end{aligned}$$

and  $U_1 - U_3$  changes sign on the interval  $(0, \frac{\pi}{2})$ . The mean value theorem implies that there is  $\hat{a} \in (0, \frac{\pi}{2})$  such that  $U_1(\hat{a}) = U_3(\hat{a})$ .

Thus, we know that  $U_1(\hat{a}) = U_2(\hat{a}) = U_3(\hat{a})$  and the identity  $x^2 + y^2 + z^2 = 1$  leads to  $U_i(\hat{a}) = \frac{1}{3}$  for  $i = 1, 2, 3$ , which matches

$$\int_{\mathbb{S}^2} x^2 = \int_{\mathbb{S}^2} y^2 = \int_{\mathbb{S}^2} z^2 = \frac{1}{3}.$$

Thus, the pair  $(\{x_S\}, \gamma_{\hat{a}})$  integrates the monomials  $x^2, y^2, z^2$  exactly. We also observe symbolically (can also be argued by symmetry) that the monomials  $xy, xz, yz$  integrate to zero, so that we obtain a hybrid 2-design. Numerically, we observe  $\hat{a} \approx 1.359$ . ■

primal and dual polytopes	$s$	$\rho$
tetrahedron	3	$\frac{4}{4+3\sqrt{2}\arccos(-\frac{1}{3})} \approx 0.33$
octahedron/cube	5	$\frac{9}{25} = 0.36$
cube/octahedron	5	$\frac{10\sqrt{2}+3\arccos(\frac{1}{3})}{10\sqrt{2}+35\arccos(\frac{1}{3})} \approx 0.31$
rhombic dodecahedron/ cuboctahedron	5	$\frac{10-3\sqrt{2}\arccos(\frac{1}{\sqrt{3}})}{10+5\sqrt{2}\arccos(\frac{1}{\sqrt{3}})} \approx 0.35$
cuboctahedron/rhombic dodecahedron	5	$\frac{21}{25} = 0.84$
icosahedron/dodecahedron	9	$\frac{126+45\arccos(\frac{1}{\sqrt{5}})}{126+301\arccos(\frac{1}{\sqrt{5}})} \approx 0.38$
dodecahedron/icosahedron	9	$\frac{1190\sqrt{5}-675\arccos(\frac{\sqrt{5}}{3})}{1190\sqrt{5}+6237\arccos(\frac{\sqrt{5}}{3})} \approx 0.30$
icosidodecahedron/rhombic triacontahedron	9	$\frac{45}{49} \approx 0.92$
rhombic triacontahedron/icosidodecahedron	9	$\frac{7(17\sqrt{5}-27)+135\arccos(\sqrt{\frac{1}{3}+\frac{2}{3\sqrt{5}}})}{7(17\sqrt{5}-27)+567\arccos(\sqrt{\frac{1}{3}+\frac{2}{3\sqrt{5}}})} \approx 0.37$

TABLE 2. Hybrid  $s$ -designs of Theorem 4.3. The primal polytope induces the geodesic cycle through its edges and the dual polytope provides the vertices.

## 4.2 Hybrid designs from pairs of dual polytopes

To improve the covering radius of a geodesic  $t$ -design cycle derived from the edges of a convex polytope in  $\mathbb{R}^3$ , one can include the midpoints of the polytope's 2-dimensional faces, projected onto the sphere. More formally, for a regular convex polytope  $\mathcal{P}$  in  $\mathbb{R}^3$ , its dual polytope  $\mathcal{P}_{\text{dual}}$  is formed by taking the convex hull of the centers of  $\mathcal{P}$ 's facets (its 2-dimensional faces). This process results in another regular convex polytope, and  $(\mathcal{P}, \mathcal{P}_{\text{dual}})$  is referred to as a dual pair. The tetrahedron is special, as it is self-dual, meaning its dual realization is a rotated version of itself.

For such a dual pair, the geodesic cycle is induced by the edges of the first (primal) polytope, while vertices originate from the second (dual) polytope. If the associated pure designs have strength  $t$ , then we expect that their hybrid use leads to a stronger hybrid  $s$ -design with  $s > t$ . The following theorem confirms this idea for the hybrid designs that are illustrated in Figures 4, 5, and 6 in the introduction.

**Theorem 4.3.** *Table 2 provides a list of primal and dual polytopes, whose edges and vertices yield hybrid  $s$ -designs on  $\mathbb{S}^2$  with the specified balancing factor  $\rho$ .*

## 5 Proof of Theorem 4.3

Our proof of Theorem 4.3 is guided by the approach in [19], where suitable group orbits are derived to get strong  $t$ -design points. The approach consists of two steps and is based on invariant theory. First, we derive an integration result for two group orbits, where one consists of points and the other of spherical arcs. Second, we analyze spherical polynomials that are invariant under the symmetry groups of



distinct pairs of dual polytopes. The combination and balancing of these steps will lead to the proof of Theorem 4.3.

### 5.1 Combining orbits of points with orbits of geodesic arcs

Lemma 2.1 enables exact integration on  $\Pi_t$  using orbits of arcs provided that the space of invariant elements  $\Pi_t^G$  is one-dimensional. If we identify  $s > t$  such that  $\Pi_s^G$  is two-dimensional, then we can still derive exact integration of  $\Pi_s$  by adding another orbit of points.

Assume the orthogonal decomposition

$$\Pi_s^G = \mathbb{R} \oplus \mathbb{R}\pi_{\text{inv}}$$

is valid, where  $\pi_{\text{inv}}$  is a suitable  $G$ -invariant polynomial. If  $x_1 \in \mathbb{S}^d$  is a root of  $\pi_{\text{inv}}$ , then the orbit  $Gx_1$  forms an  $s$ -design, see [41]. The subset of the sphere where  $\pi_{\text{inv}}$  vanishes has measure zero, so that the random choice of  $x_1$  with respect to the surface measure of the sphere fails with probability one.

We overcome this limitation by introducing an additional orbit of arcs. This approach effectively reverses the situation, making the construction work for almost all points, except for a set of measure zero. Our method parallels McLaren's strategy in [35], see also [19], which employs multiple point orbits for weighted quadrature formulas.

**Lemma 5.1.** *Suppose that  $G \subseteq \mathcal{O}(d+1)$  is a finite group such that  $\Pi_s^G$  is two-dimensional, so that there is  $\pi_{\text{inv}} \in \Pi_s^G$  satisfying the orthogonal decomposition*

$$\Pi_s^G = \mathbb{R} \oplus \mathbb{R}\pi_{\text{inv}}.$$

Given an arc  $\gamma_1 \subseteq \mathbb{S}^d$ , define the set  $\mathcal{N} = \{x \in \mathbb{S}^d : \pi_{\text{inv}}(x) = \frac{1}{\ell(\gamma_1)} \int_{\gamma_1} \pi_{\text{inv}}\}$ .

(a) Then for all  $x_1 \in \mathbb{S}^d \setminus \mathcal{N}$  there is a factor  $\rho \in \mathbb{R}$  such that

$$(5) \quad \frac{\rho}{|G|} \sum_{g \in G} \pi(gx_1) + \frac{1-\rho}{|G|} \sum_{g \in G} \frac{1}{\ell(\gamma_1)} \int_{g\gamma_1} \pi = \int_{\mathbb{S}^d} \pi, \quad \text{for all } \pi \in \Pi_s.$$

(b) Moreover, there is  $x_1 \in \mathbb{S}^d$  such that  $\pi_{\text{inv}}(x_1)$  and  $\frac{1}{\ell(\gamma_1)} \int_{\gamma_1} \pi_{\text{inv}}$  have opposite signs and then (5) holds with a balancing factor that satisfies  $0 \leq \rho < 1$ .

*Proof.* (a) For all  $x_1 \in \mathbb{S}^d \setminus \mathcal{N}$ , the definition of  $\mathcal{N}$  yields

$$\pi_{\text{inv}}(x_1) \neq \frac{1}{\ell(\gamma_1)} \int_{\gamma_1} \pi_{\text{inv}}.$$

Thus, their difference is nonzero and, hence, there is some  $\rho \in \mathbb{R}$  satisfying the identity

$$(6) \quad \rho \left( \pi_{\text{inv}}(x_1) - \frac{1}{\ell(\gamma_1)} \int_{\gamma_1} \pi_{\text{inv}} \right) = -\frac{1}{\ell(\gamma_1)} \int_{\gamma_1} \pi_{\text{inv}}.$$

Since  $\pi_{\text{inv}}$  is orthogonal to the constants, we have  $\int_{\mathbb{S}^d} \pi_{\text{inv}} = 0$ , and (6) may be stated as

$$\rho \pi_{\text{inv}}(x_1) + \frac{1-\rho}{\ell(\gamma_1)} \int_{\gamma_1} \pi_{\text{inv}} = \int_{\mathbb{S}^d} \pi_{\text{inv}}.$$

Let  $\pi \in \Pi_s$ . Since the space of invariant polynomials  $\Pi_s^G = \mathbb{R} \oplus \mathbb{R}\pi_{\text{inv}}$  has dimension two, the invariant polynomial  $\pi^G = \frac{1}{|G|} \sum_{g \in G} \pi \circ g$  can be written as a linear combination  $\pi^G = r_0 + r_1 \pi_{\text{inv}}$  for some  $r_0, r_1 \in \mathbb{R}$ . The summation over the group in (5) leads to

$$\begin{aligned}
\frac{\rho}{|G|} \sum_{g \in G} \pi(gx_1) + \frac{1-\rho}{|G|} \sum_{g \in G} \frac{1}{\ell(\gamma_1)} \int_{g\gamma_1} \pi &= \rho \pi^G(x_1) + \frac{1-\rho}{\ell(\gamma_1)} \int_{\gamma_1} \pi^G \\
&= \rho r_0 + \rho r_1 \pi_{\text{inv}}(x_1) + (1-\rho)r_0 + \frac{1-\rho}{\ell(\gamma_1)} r_1 \int_{\gamma_1} \pi_{\text{inv}} \\
&= r_0 + r_1 \left( \rho \pi_{\text{inv}}(x_1) + \frac{1-\rho}{\ell(\gamma_1)} \int_{\gamma_1} \pi_{\text{inv}} \right) \\
&= r_0 + r_1 \int_{\mathbb{S}^d} \pi_{\text{inv}} \\
&= \int_{\mathbb{S}^d} \pi^G \\
&= \int_{\mathbb{S}^d} \pi,
\end{aligned}$$

where the last equality follows from the orthogonal invariance of the measure on  $\mathbb{S}^d$ . This completes the proof of the first part of the theorem.

(b) To verify the second part, we first assume that  $\frac{1}{\ell(\gamma_1)} \int_{\gamma_1} \pi_{\text{inv}} \neq 0$ . Since  $\pi_{\text{inv}}$  is orthogonal to the constants, it necessarily assumes both positive and negative values. Thus, there is  $x_1 \in \mathbb{S}^d$  such that  $\pi_{\text{inv}}(x_1)$  and  $\frac{1}{\ell(\gamma_1)} \int_{\gamma_1} \pi_{\text{inv}}$  have opposite signs. The choice

$$(7) \quad \rho = \frac{-\frac{1}{\ell(\gamma_1)} \int_{\gamma_1} \pi_{\text{inv}}}{\pi_{\text{inv}}(x_1) - \frac{1}{\ell(\gamma_1)} \int_{\gamma_1} \pi_{\text{inv}}}$$

implies  $0 < \rho < 1$  and leads to (6). Thus, the integration condition (5) holds.

If  $\frac{1}{\ell(\gamma_1)} \int_{\gamma_1} \pi_{\text{inv}} = 0$ , then (5) holds for  $\rho = 0$  and all  $x_1 \in \mathbb{S}^d$ . Alternatively, we may choose  $x_1$  as a root of  $\pi_{\text{inv}}$  and then (5) holds for all  $\rho \in \mathbb{R}$ . In any case, this completes the proof of the second part of the theorem.  $\blacksquare$

To prove Theorem 4.3 as a consequence of Lemma 5.1, we still need some observations from invariant theory, and we will later specify both  $x_1$  and  $\gamma_1$  such that  $\pi_{\text{inv}}(x_1)$  and  $\frac{1}{\ell(\gamma_1)} \int_{\gamma_1} \pi_{\text{inv}}$  have opposite signs

## 5.2 Hybrid designs and invariant polynomials on the sphere

To apply Lemma 5.1, we must check that  $\Pi_s^G = \mathbb{R} \oplus \mathbb{R}\pi_{\text{inv}}$ . In particular, we seek the maximal  $s$  such that  $\Pi_s^G$  is two-dimensional.

For preparation, we recall the harmonic decomposition of polynomials on the sphere, cf. [44]. Let  $\mathcal{H}_l$  be the vector space of spherical harmonics of degree  $l \in \mathbb{N}$ . These are exactly the restrictions to  $\mathbb{S}^d$  of the homogeneous harmonic polynomials of degree  $l$  in  $d+1$  variables. Each space  $\mathcal{H}_l$  is invariant under the orthogonal group

$\mathcal{O}(d+1)$ , and the polynomials  $\Pi_s$  on  $\mathbb{S}^d$  are orthogonally decomposed into

$$\Pi_s = \bigoplus_{l=0}^s \mathcal{H}_l.$$

To find the invariant polynomials  $\Pi_s^G = \bigoplus_{l=0}^s \mathcal{H}_l^G$ , we can analyze each component  $\mathcal{H}_l^G$  individually for  $l = 0, \dots, s$ .

The dimensions  $\dim(\mathcal{H}_l^G)$  are calculated via Molien's Theorem as follows. The harmonic decomposition  $\bigoplus_{l \in \mathbb{N}} \mathcal{H}_l^G$  of the  $G$ -invariant polynomials gives rise to the (harmonic) Molien series

$$\mathcal{M}(\omega) = \sum_{l \in \mathbb{N}} \dim(\mathcal{H}_l^G) \omega^l,$$

cf. [19, 36]. Molien's Theorem as derived in [36] for the spherical harmonics states that this series can be written as the finite sum

$$\mathcal{M}(\omega) = \frac{1}{|G|} \sum_{g \in G} \frac{1 - \omega^2}{\det(\mathbb{I}_{d+1} - \omega g)}.$$

The factor  $1 - \omega^2$  appears because we are not dealing with general homogeneous polynomials on  $\mathbb{R}^{d+1}$  but spaces of spherical harmonics as explained in [36, Section III].

For the tetrahedral group  $T_d = A_3$ , the octahedral group  $O_h = B_3$ , and the icosahedral group  $I_h = H_3$ , the Molien series are

$$\begin{aligned} \mathcal{M}_{T_d}(\omega) &= \frac{1}{(1 - \omega^3)(1 - \omega^4)} = 1 + \omega^3 + \omega^4 + O(\omega^6), \\ \mathcal{M}_{O_h}(\omega) &= \frac{1}{(1 - \omega^4)(1 - \omega^6)} = 1 + \omega^4 + \omega^6 + O(\omega^8), \\ \mathcal{M}_{I_h}(\omega) &= \frac{1}{(1 - \omega^6)(1 - \omega^{10})} = 1 + \omega^6 + \omega^{10} + O(\omega^{12}), \end{aligned}$$

cf. [19, 36], see also [27, Table 1 in Section 3.7, (20) in Section 3.8]. This leads to the following observations.

**Lemma 5.2.** *The spaces  $\mathcal{H}_3^{T_d}$ ,  $\mathcal{H}_4^{O_h}$ ,  $\mathcal{H}_6^{I_h}$  are one-dimensional and we have the decompositions*

$$\Pi_3^{T_d} = \mathbb{R} \oplus \mathcal{H}_3^{T_d}, \quad \Pi_5^{O_h} = \mathbb{R} \oplus \mathcal{H}_4^{O_h}, \quad \Pi_9^{I_h} = \mathbb{R} \oplus \mathcal{H}_6^{I_h}.$$

While formulated differently, the claims of this lemma were already known to Meyer [36] in 1954, see also Sobolev [42] in 1962 and McLaren [35] in 1963. They directly imply

$$\dim(\Pi_3^{T_d}) = \dim(\Pi_5^{O_h}) = \dim(\Pi_9^{I_h}) = 2.$$

Moreover, these are the highest degrees, 3, 5, and 9, respectively, such that the invariant spaces are two-dimensional.

According to Lemma 5.2, the assumption of Lemma 5.1 is satisfied for the respective group  $G$  and polynomial degree  $s$ . There is some  $G$ -invariant polynomial  $\pi_{\text{inv}} \in \Pi_s^G$  such that  $\Pi_s^G = \mathbb{R} \oplus \mathbb{R}\pi_{\text{inv}}$ . To compute the balancing factor  $\rho$ , however,

we still need to determine the basis element  $\pi_{\text{inv}}$  for each of the spaces  $\mathcal{H}_3^{T_d}$ ,  $\mathcal{H}_4^{O_h}$ , and  $\mathcal{H}_6^{I_h}$ .

**Remark 5.1.** If the polytope  $\mathcal{P}$  is transformed by some orthogonal matrix  $O \in O(3)$ , so that the new realization is given by  $\tilde{\mathcal{P}} := O\mathcal{P}$ , then its symmetry group becomes  $\tilde{G} = OGO^*$ . The dimensions of the invariant polynomial spaces do not change, but the invariant polynomial  $\tilde{\pi}_{\text{inv}}$  undergoes the orthogonal transformation  $\tilde{\pi}_{\text{inv}} = \pi_{\text{inv}} \circ O^*$ . Thus, to determine  $\pi_{\text{inv}}$ , we need to specify a particular representation of the symmetry group and implicitly a realization of the associated primal and dual polytopes.

For the (full) octahedral group  $O_h = B_3$ , we use the 48 matrices that permute the three coordinates and multiply an arbitrary number of the coordinates by  $-1$ . The tetrahedral group  $T_d = A_3$  consists of 24 matrices that form a subgroup of  $O_h$ , where not all but only an even number of coordinates is multiplied by  $-1$ .

The icosahedral group  $I_h = H_3$  consists of 120 matrices and contains the 12 rotations in  $T_d$ , the 9 reflections  $I_3 - \frac{2}{\|v\|^2}vv^\top$  in  $O_h$  for  $v = (1, 0, 0)^\top$ ,  $v = (0, 1, 0)^\top$ ,  $v = (0, 0, 1)^\top$ ,  $v = (\pm 1, 1, 0)^\top$ ,  $v = (\pm 1, 0, 1)^\top$ , and  $v = (0, \pm 1, 1)^\top$ , and the additional reflections for  $v = (\pm\phi, \pm\phi^{-1}, \pm 1)^\top$ ,  $v = (\pm 1, \pm\phi, \pm\phi^{-1})^\top$ , and  $v = (\pm\phi^{-1}, \pm 1, \pm\phi)^\top$ , where all sign combinations are allowed and  $\phi = \frac{1+\sqrt{5}}{2}$  is the golden ratio.

*Proof of Theorem 4.3.* (i) The polynomial  $\pi_{\text{inv}}$  of degree three invariant under the tetrahedral group  $T_d$  is  $\pi_{\text{inv}}(x, y, z) = xyz$ , cf. [19, 36] and generates  $\mathcal{H}_3^{T_d} = \mathbb{R}\pi_{\text{inv}}$ .

A spherical arc  $\gamma_1$  is induced by an edge of the primal realization of the tetrahedron that is given by the vertices  $\frac{1}{\sqrt{3}}(1, 1, 1)$ ,  $\frac{1}{\sqrt{3}}(1, -1, -1)$ ,  $\frac{1}{\sqrt{3}}(-1, 1, -1)$ , and  $\frac{1}{\sqrt{3}}(-1, -1, 1)$ . We also pick a vertex  $x_1 = \frac{1}{\sqrt{3}}(1, 1, -1)$  of the tetrahedron's dual realization. Direct computations lead to

$$\pi_{\text{inv}}(x_1) = -\frac{1}{3\sqrt{3}}, \quad \frac{1}{\ell(\gamma_1)} \int_{\gamma_1} \pi_{\text{inv}} = \frac{2\sqrt{2}}{9\sqrt{3} \arccos(-\frac{1}{3})},$$

and we recognize that the two values have opposite signs. Hence, the assumptions of Lemma 5.1 are satisfied, and we determine the balancing factor  $\rho$  according to (7) by

$$\rho = \frac{-\frac{2\sqrt{2}}{9\sqrt{3} \arccos(-\frac{1}{3})}}{-\frac{1}{3\sqrt{3}} - \frac{2\sqrt{2}}{9\sqrt{3} \arccos(-\frac{1}{3})}} = \frac{4}{4 + 3\sqrt{2} \arccos(-\frac{1}{3})} \approx 0.33.$$

(ii - v) The polynomial  $x^4 + y^4 + z^4$  is invariant under the octahedral group  $O_h$  [36], and, according to  $\int_{\mathbb{S}^2} x^4 + y^4 + z^4 = \frac{3}{5}$ , we deduce that  $\pi_{\text{inv}}(x, y, z) = x^4 + y^4 + z^4 - \frac{3}{5}$  generates  $\mathcal{H}_4^{O_h} = \mathbb{R}\pi_{\text{inv}}$ .

We apply Lemma 5.1 and observe in Mathematica that the condition (6) on  $\rho$  is solvable by (7) for the respective roles of the cube and the octahedron as well as the rhombic dodecahedron and the cuboctahedron. Symbolic calculations lead to the values of  $\rho$  provided in Table 2.

(vi-ix) For the icosahedral group  $I_h$ , the following invariant polynomial

$$\pi_0(x, y, z) = (\phi^2 x^2 - y^2)(\phi^2 y^2 - z^2)(\phi^2 z^2 - x^2), \quad \phi = \frac{1+\sqrt{5}}{2},$$

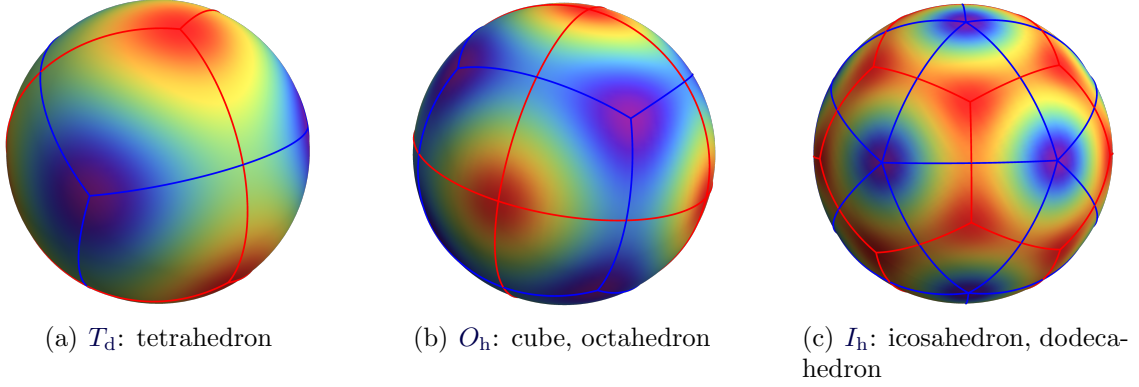


FIGURE 8. The invariant polynomial  $\pi_{\text{inv}}$  is shown for  $G = T_d, O_h,$  and  $I_h$  with the rainbow color scheme that ranges from  $\min \pi_{\text{inv}}$  (violet) to  $\max \pi_{\text{inv}}$  (red). The vertices of the associated pairs of convex regular polytopes (blue, red) lie precisely at the minima and maxima, respectively.

is provided in [36]. We may compute  $\int_{\mathbb{S}^2} \pi_0 = -\frac{2+\sqrt{5}}{21}$ , so that  $\pi_{\text{inv}} := \pi_0 + \frac{2+\sqrt{5}}{21}$  generates  $\mathcal{H}_6^{I_h} = \mathbb{R}\pi_{\text{inv}}$ .

The balancing factor  $\rho$  is determined according to (7) by the computer algebra system for the icosahedron and the dodecahedron as well as the icosidodecahedron and the rhombic triacontahedron that leads to the values of  $\rho$  provided in Table 2. ■

**Remark 5.2.** The invariant polynomials  $\pi_{\text{inv}}$  as derived in the proof of Theorem 4.3 are shown in Figure 8. The maximum and the minimum are attained precisely at the vertices of the associated convex regular polytopes.

We conclude our discussion of hybrid designs in  $\mathbb{S}^2$  and now turn our attention to higher dimensions.

## 6 Hybrid designs in higher dimensions

We first derive our strongest hybrid designs that are valid in arbitrary dimensions. Then, we focus on  $\mathbb{S}^3$  and ultimately obtain the strongest hybrid design overall.

**Proposition 6.1.** *The  $d$ -octahedron and the  $d$ -cube are a dual polytope pair that provides hybrid 5-designs in  $\mathbb{S}^{d-1}$ .*

- (a) *If the geodesic cycle is induced by the edges of the  $d$ -octahedron, and the vertices are taken from its dual  $d$ -cube, then the balancing factor is*

$$\rho_{\text{oct/cube}} = \frac{3d(d-2)}{3d^2 + 2d - 8}.$$

- (b) *For the reverse roles, the balancing factor is*

$$\rho_{\text{cube/oct}} = 3 \cdot \frac{d-2}{d+2} \cdot \frac{2(d-2)\sqrt{d-1} - d(d-4) \arccos\left(\frac{d-2}{d}\right)}{6(d-2)\sqrt{d-1} + d(5d-8) \arccos\left(\frac{d-2}{d}\right)}.$$

*Proof.* The symmetry group of the  $d$ -cube and the  $d$ -octahedron is the finite Coxeter group  $B_d$ . According to [19], see also [27, Table 1 in Section 3.7, (20) in Section 3.8], [36], its Molien series is

$$\mathcal{M}_{B_d}(\omega) = (1 - \omega^4)^{-1}(1 - \omega^6)^{-1} \cdots (1 - \omega^{2d})^{-1} = 1 + \omega^4 + \omega^6 + O(\omega^8).$$

Hence,  $\mathcal{H}_4^{B_d}$  is one-dimensional and the space of  $B_d$ -invariant polynomials of degree at most 5 is  $\Pi_5^{B_d} = \mathbb{R} \oplus \mathcal{H}_4^{B_d}$ .

The root system of  $B_d$  is  $\pm e_i$  and  $\pm e_i \pm e_j$ , for  $1 \leq i < j \leq d$ , so that  $B_d$  is generated by the associated reflections  $I_d - \frac{2}{\|v\|^2}vv^\top$ , where  $v$  runs through the roots. We may deduce that the polynomial  $x_1^4 + \dots + x_d^4$  is  $B_d$ -invariant. Since  $\int_{\mathbb{S}^{d-1}} x_1^4 + \dots + x_d^4 = \frac{3}{d+2}$ , the  $B_d$ -invariant polynomial  $\pi_{\text{inv}}$  that spans  $\mathcal{H}_4^{B_d} = \mathbb{R}\pi_{\text{inv}}$  is

$$\pi_{\text{inv}}(x_1, \dots, x_d) = x_1^4 + \dots + x_d^4 - \frac{3}{d+2}.$$

(a) To determine  $\rho_{\text{oct}/\text{cube}}$ , we choose  $x_1 = \frac{1}{\sqrt{d}}(1, \dots, 1)$  as the vertex of the  $d$ -cube and observe  $\pi_{\text{inv}}\left(\frac{1}{\sqrt{d}}(1, \dots, 1)\right) = -\frac{2(d-1)}{d(d+2)}$ . The arc derived from the edge of the  $d$ -octahedron is  $\gamma_{e_1, e_2} = \sin\left(\frac{\pi}{2} - s\right)e_1 + \sin(s)e_2$ , for  $s \in [0, \frac{\pi}{2}]$ . Direct computations lead to

$$\frac{1}{\ell(\gamma_{e_1, e_2})} \int_{\gamma_{e_1, e_2}} \pi_{\text{inv}} = \frac{3(d-2)}{4(d+2)}.$$

We compute the balancing factor by (7) and obtain

$$\rho_{\text{oct}/\text{cube}} = \frac{3d(d-2)}{3d^2 + 2d - 8}.$$

(b) To determine  $\rho_{\text{cube}/\text{oct}}$ , we observe  $\pi_{\text{inv}}(e_1) = \frac{d-1}{d+2}$ . For the integration along an arc  $\gamma_{x,y}$  induced by the edge of the cube from  $x = \frac{1}{\sqrt{d}}(-1, 1, \dots, 1)^\top$  to  $y = \frac{1}{\sqrt{d}}(1, 1, \dots, 1)^\top$ , we get help from Mathematica and eventually derive the balancing factor as claimed. ■

The remaining section is dedicated to derive explicit hybrid designs in  $\mathbb{S}^3$  from the six convex regular polytopes in  $\mathbb{R}^4$ . The symmetry group of the cube-octahedron pair in  $\mathbb{R}^4$  is  $B_4$ , it yields a hybrid 5-design, and the balancing factors in Proposition 6.1 simplify to

$$\rho_{\text{cube}/\text{oct}} = \frac{3\sqrt{3}}{3\sqrt{3} + 4\pi} \approx 0.29, \quad \rho_{\text{oct}/\text{cube}} = \frac{1}{2}.$$

The symmetries of the remaining four convex regular polytopes are the finite reflection groups  $A_4$ ,  $F_4$  and  $H_4$ . We derive from [19] that their Molien series satisfy



$$\begin{aligned}
\mathcal{M}_{A_4}(\omega) &= (1 - \omega^3)^{-1}(1 - \omega^4)^{-1}(1 - \omega^5)^{-1} &= 1 + \omega^3 + \omega^4 + O(\omega^5), \\
\mathcal{M}_{F_4}(\omega) &= (1 - \omega^6)^{-1}(1 - \omega^8)^{-1}(1 - \omega^{12})^{-1} &= 1 + \omega^6 + \omega^8 + O(\omega^{12}), \\
\mathcal{M}_{H_4}(\omega) &= (1 - \omega^{12})^{-1}(1 - \omega^{20})^{-1}(1 - \omega^{30})^{-1} &= 1 + \omega^{12} + \omega^{20} + O(\omega^{24}).
\end{aligned}$$

The symmetry group of the self-dual 4-dimensional tetrahedron (the 4-dimensional regular simplex) is  $A_4$  and satisfies  $\Pi_3^{A_4} = \mathbb{R} \oplus \mathcal{H}_3^{A_4}$ , where  $\mathcal{H}_3^{A_4}$  is one-dimensional. It gives rise to a hybrid 3-design and to determine the balancing factor  $\rho_{tetra}$ , we invoke some help from Mathematica and obtain

$$\rho_{tetra} = \frac{1}{1 + \frac{9\sqrt{3}}{8\sqrt{5}} \arccos(-\frac{1}{4})} \approx 0.39.$$

Analogously, the self-dual 24-cell, whose symmetry group  $F_4$  has 1152 elements, see [19] for invariants, induces a hybrid 7-design. Symbolic calculus leads to the balancing factor  $\rho_{24} = \frac{5}{14}$ .

The symmetry group of the 120-cell and 600-cell is the exceptional group  $H_4$  with 14400 elements. Individually, these polytopes induce pure 11-designs as points or geodesic cycles. We realize the two polytopes as a dual pair and now derive the strongest hybrid design so far.

**Theorem 6.2.** *Let  $\gamma$  be the geodesic cycle derived from the edges of the 600-cell and  $X$  be the vertices of the 120-cell. Then  $(\gamma, X)$  is a hybrid 19-design with balancing factor  $\rho_{600/120} = \frac{176}{301} \approx 0.58$ .*

*Proof.* The 600-cell is edge-transitive, so that  $\gamma$  is an orbit of an arc  $\gamma_1$  under  $G = H_4$  induced by a single edge. The invariant space  $\Pi_{19}^{H_4} = \mathbb{R} \oplus \mathcal{H}_{12}^{H_4}$  is two-dimensional [19]. Hence, the assumption of Lemma 5.1 is satisfied and there are  $x_1 \in \mathbb{S}^3$  and  $0 < \rho < 1$  such that the integration conditions (5) hold for  $\Pi_{19}$  and, hence,  $(\gamma, Gx_1)$  is a hybrid 19-design.

To verify that  $x_1$  can be chosen as a vertex of the 120-cell, so that  $|X| = 600$ , we must derive an explicit expression of the invariant polynomial  $\pi_{\text{inv}} \in \mathcal{H}_{12}^{H_4}$ , where  $H_4$  is represented as a finite subgroup of the orthogonal group  $\mathcal{O}(4)$ . However, we were neither successful through literature search nor through any computer algebra system as those commonly use a different representation of  $H_4$  that is not contained in  $\mathcal{O}(4)$ .

Therefore, we compute  $\pi_{\text{inv}}$  ourselves. We pick the 120 vertices of the 600-cell as the root system of  $H_4$  given by 16 vertices  $\frac{1}{2}(\pm 1, \pm 1, \pm 1, \pm 1)^\top$ , 8 vertices by all permutations of  $(\pm 1, 0, 0, 0)^\top$ , and 96 vertices by all even permutations of  $\frac{1}{2}(\pm\phi, \pm 1, \pm\frac{1}{\phi}, 0)^\top$ , cf. [12], [11, Section 8.7]. These vectors induce 120 reflection matrices  $I_4 - 2vv^\top$  that we have used to generate all 14400 matrices of  $H_4$  in Mathematica. This was easier said than done but we eventually succeeded.

For the three-sphere  $\mathbb{S}^3$ , the dimension of  $\mathcal{H}_l$  is  $\dim(\mathcal{H}_l) = (l + 1)^2$ , and the spherical harmonics  $Y_{l,m}$  of degree  $l$  provide an orthonormal basis for  $\mathcal{H}_l$ , so that

$$\mathcal{H}_l = \text{span}\{Y_{l,m} : m = 1, \dots, (l + 1)^2\}.$$

To identify the invariant polynomial  $\pi_{\text{inv}}$ , we recall that the Gegenbauer polynomials  $C_l^{(\alpha)}$  with  $\alpha = 1$ , normalized by  $C_l^{(\alpha)}(1) = 1$ , satisfy the addition formula of spherical harmonics

$$(l+1)^2 C_l^{(1)}(\langle a, b \rangle) = \sum_{m=1}^{(l+1)^2} Y_{l,m}(a) Y_{l,m}(b), \quad a, b \in \mathbb{S}^3.$$

Therefore, the space  $\mathcal{H}_l$  is spanned by  $\text{span}\{b \mapsto C_l^{(1)}(\langle a, b \rangle) : a \in \mathbb{S}^3\} = \mathcal{H}_l$ . In particular, the group average of  $C_{12}^{(1)}(\langle a, \cdot \rangle)$  is contained in  $\mathcal{H}_{12}^{H_4}$ , for all  $a \in \mathbb{S}^3$ , and we have computed  $\pi_{\text{inv}} \in \mathcal{H}_{12}^{H_4}$  by summing

$$\pi_{\text{inv}}(q) := \frac{1}{14400} \sum_{g \in H_4} C_{12}^{(1)}\left(\left\langle \begin{pmatrix} 1 \\ 0 \\ 0 \\ 0 \end{pmatrix}, g \begin{pmatrix} q_1 \\ q_2 \\ q_3 \\ q_4 \end{pmatrix} \right\rangle\right), \quad q \in \mathbb{S}^3,$$

in Mathematica.

The arc  $\gamma_1$  is induced by the edge between  $(1, 0, 0, 0)^\top$  and  $\frac{1}{2}(\phi, 1, \frac{1}{\phi}, 0)^\top$  of the 600-cell, and we pick  $x_1 = (0, 0, \frac{1}{\sqrt{2}}, \frac{1}{\sqrt{2}})^\top$  as a vertex of the 120-cell. Remarkably, symbolic calculations in Mathematica deliver simple rational expressions for

$$\frac{1}{\ell(\gamma_1)} \int_{\gamma_1} \pi_{\text{inv}} = \frac{11}{25}, \quad \pi_{\text{inv}}(x_1) = -\frac{5}{16},$$

that lead to the balancing factor  $\rho_{600/120} = \frac{-\frac{11}{25}}{-\frac{5}{16} - \frac{11}{25}} = \frac{176}{301}$ . ■

Theorem 6.2 yields an exceptionally strong hybrid design. Unlike most spherical 19-designs in the literature, which are typically derived via numerical procedures on  $\mathbb{S}^2$  and  $\mathbb{S}^3$  [21, 24, 52] and therefore lack a rigorous proof, this design is explicitly given as a group orbit. To the best of our knowledge, the only other comparable spherical 19-design is presented in [19] as the (point) orbit  $Gx_1$ , where  $G = H_4$  and  $x_1 \in \mathbb{S}^3$  is such that  $\pi_{\text{inv}}(x_1) = 0$ . According to [19], the smallest of those orbits consists of 1440 points. The hybrid 19-design in Theorem 6.2 for comparison is built from 720 geodesic arcs and 600 points.

## 7 The basic idea behind exact integration via invariants

We have used invariants for exact integration in  $\Pi_t$  by assuming  $\dim(\Pi_t^G) = 1$  in Lemma 2.1 and  $\dim(\Pi_t^G) = 2$  in Lemma 5.1. We now explain the main idea behind using invariants to derive exact integration formulas, which holds regardless of the dimension  $\dim(\Pi_t^G)$ . This idea becomes even more evident when we explore it in a broader, more general setting. Instead of restricting ourselves to points or curves, we start with a signed measure  $\mu$  on the sphere  $\mathbb{S}^d$ . The support of  $\mu$  could include points, arcs, curves, or other structures.

Let  $G$  be a closed subgroup of the orthogonal group  $\mathcal{O}(d+1)$ , which need not be finite. The space of  $G$ -invariant polynomials of degree at most  $t$  is still denoted by  $\Pi_t^G$ . Since  $G$  is equipped with the normalized Haar measure  $\sigma_G$ , consistent with earlier sections, summation is simply replaced by integration, and we define the

$G$ -average of a polynomial  $\pi \in \Pi_t$  as

$$\pi^G := \int_G \pi \circ g \, d\sigma_G(g).$$

This ensures that  $\pi^G$  is  $G$ -invariant. Since  $\int_{\mathbb{S}^d} \pi \circ g(x) \, d\mu(x) = \int_{\mathbb{S}^d} \pi(x) \, d(g_*\mu)(x)$ , where  $g_*\mu$  is the pushforward measure, the averaging process makes also sense for  $\mu$  by defining  $\mu^G$  as the average over the pushforwards  $g_*\mu$ , so that we define

$$(8) \quad \mu^G := \int_G g_*\mu \, d\sigma_G(g).$$

This produces a  $G$ -invariant measure  $\mu^G$  and leads to the following key observation about the connection between invariant theory and exact integration.

**Proposition 7.1.** *The signed measure  $\mu$  integrates  $\Pi_t^G$  exactly if and only if  $\mu^G$  integrates  $\Pi_t$  exactly.*

*Proof.* The abstract definition (8) taken in the weak sense means that  $\mu^G$  satisfies

$$\begin{aligned} \int_{\mathbb{S}^d} \pi(x) \, d\mu^G(x) &= \int_G \int_{\mathbb{S}^d} \pi(x) \, dg_*\mu(x) \, d\sigma_G(g) \\ &= \int_G \int_{\mathbb{S}^d} \pi \circ g(x) \, d\mu(x) \, d\sigma_G(g) \\ &= \int_{\mathbb{S}^d} \pi^G(x) \, d\mu(x), \end{aligned}$$

where the last equality is due to Fubini's theorem. Since the measure on the sphere is orthogonally invariant, we also have  $\int_{\mathbb{S}^d} \pi^G = \int_{\mathbb{S}^d} \pi$ . Hence, the equality  $\int_{\mathbb{S}^d} \pi^G(x) \, d\mu(x) = \int_{\mathbb{S}^d} \pi^G$  holds if and only if  $\int_{\mathbb{S}^d} \pi(x) \, d\mu^G(x) = \int_{\mathbb{S}^d} \pi$  is satisfied. ■

We are ultimately seeking exact integration of  $\Pi_t$ . The benefit of Proposition 7.1 is that identifying a measure  $\mu$  that integrates  $\Pi_t^G$  exactly is easier than  $\Pi_t$ , because the space of invariant polynomials is smaller. In the extreme case  $\Pi_t^G = \mathbb{R}$ , every probability measure  $\mu$  works.

To make the connection to Lemma 5.1, take  $x_1 \in \mathbb{S}^d$  and a geodesic arc  $\gamma_1$ . Let  $\delta_{x_1}$  denote the point measure and  $\nu_{\gamma_1}$  the normalized Hausdorff measure on the arc. If  $G$  is finite and the probability measure  $\mu$  is defined by

$$\mu = \rho\delta_{x_1} + (1 - \rho)\nu_{\gamma_1},$$

then the integration  $\int_{\mathbb{S}^d} \pi(x) \, d\mu^G(x)$  coincides with the left-hand-side of (5) in Lemma 5.1. Thus, Proposition 7.1 can be viewed as the general framework in which Lemmas 2.1 and 5.1 operate.

In the previous sections, our key approach was to work with groups  $G$  and degrees  $t$  for which the space of invariant polynomials  $\Pi_t^G$  is sufficiently simple, namely either one- or two-dimensional. This simplicity facilitated the construction of  $\mu$  that integrates  $\Pi_t^G$  exactly, which then led to the desired exact integration of  $\Pi_t$ . The edge-transitive polytopes were used to control the support of the invariant measure  $\mu^G$ , so that the one-dimensional part of the support did not consist of multiple disconnected arcs but was the connected path of a continuous closed curve.

## Acknowledgments

The author would like to thank Karlheinz Gröchenig, Martin Winter, and Clemens Karner for helpful discussions and comments.

## References

- [1] C. Bachoc, R. Coulangeon, and G. Nebe. Designs in Grassmannian spaces and lattices. *J. Algebraic Combinatorics*, 16:5–19, 2002.
- [2] C. Bachoc, E. Bannai, and R. Coulangeon. Codes and designs in Grassmannian spaces. *Discrete Mathematics*, 277:15–28, 2004.
- [3] B. Bajnok. Construction of designs on the 2-sphere. *Eur. J. Comb.*, 12(5):377–382, 1991.
- [4] E. Bannai. Spherical  $t$ -designs that are orbits of finite groups. *J. Math. Soc. Japan*, 36(2):341–354, 1984.
- [5] A. Bondarenko, D. Radchenko, and M. Viazovska. Optimal asymptotic bounds for spherical designs. *Ann. Math.*, 178(2):443–452, 2013.
- [6] A. Bondarenko, D. Radchenko, and M. Viazovska. Well-separated spherical designs. *Constr. Approx.*, 41(1):93–112, 2015.
- [7] P. Boyvalenkov and D. Danev. Uniqueness of the 120-point spherical 11-design in four dimensions. *Arch. Math.*, 77:360–368, 2001.
- [8] L. Brandolini, C. Choirat, L. Colzani, G. Gigante, R. Seri, and G. Travaglini. Quadrature rules and distribution of points on manifolds. *Annali della Scuola Normale Superiore di Pisa - Classe di Scienze*, XIII(4):889–923, 2014.
- [9] J. S. Brauchart, E. B. Saff, I. H. Sloan, and R. S. Womersley. QMC designs: Optimal order quasi Monte Carlo integration schemes on the sphere. *Math. Comp.*, 83:2821–2851, 2014.
- [10] A. Breger, M. Ehler, and M. Gräf. Points on manifolds with asymptotically optimal covering radius. *J. Complexity*, 48:1–14, 2018.
- [11] H. S. M. Coxeter. Regular Polytopes. *Dover Publications*, New York, 1973.
- [12] H. S. M. Coxeter. Regular and semi-regular polytopes. II *Math. Z.*, 188:559–591, 1985.
- [13] P. de la Harpe and C. Pache. Spherical designs and finite group representations (some results of E. Bannai). *Eur. J. Comb.*, 25:213–227, 2004.
- [14] P. Delsarte, J. M. Goethals, and J. J. Seidel. Spherical codes and designs. *Geom. Dedicata*, 6:363–388, 1977.
- [15] M. Ehler, M. Gräf, S. Neumayer, and G. Steidl. Curve based approximation of measures on manifolds by discrepancy minimization. *Found. Comput. Math.*, 2021.
- [16] M. Ehler and K. Gröchenig.  $t$ -design curves and mobile sampling on the sphere. *Forum of Mathematics, Sigma*, 11, 2023.
- [17] M. Ehler, K. Gröchenig, and C. Karner. Geodesic cycles on the sphere:  $t$ -designs and Marcinkiewicz-Zygmund inequalities. *arXiv:2501.06120*, 2025.
- [18] U. Etayo, J. Marzo, and J. Ortega-Cerdà. Asymptotically optimal designs on compact algebraic manifolds. *Monatsh. Math.*, 186(2):235–248, 2018.
- [19] J. M. Goethals and J. J. Seidel. Cubature formulae, polytopes, and spherical designs. In: *Davis, C., Grünbaum, B., Sherk, F.A. (eds) The Geometric Vein*. Springer, New York, NY 202–218, 1981.
- [20] F. Göring and M. Winter. The edge-transitive polytopes that are not vertex-transitive. *Ars Math. Contemp.*, 23(2), 2023.
- [21] M. Gräf and D. Potts. On the computation of spherical designs by a new optimization approach based on fast spherical Fourier transforms. *Numer. Math.*, 119:699–724, 2011.
- [22] K. Gröchenig, J. L. Romero, J. Unnikrishnan, and M. Vetterli. On minimal trajectories for mobile sampling of bandlimited fields. *Appl. Comput. Harmon. Anal.*, 39(3):487–510, 2015.
- [23] B. Grünbaum. Convex Polytopes. *Springer Science & Business Media*, 221, 2013.
- [24] R. H. Hardin and N. J. A. Sloane. McLaren’s improved snub cube and other new spherical designs in three dimensions. *Discrete Comput. Geom.*, 15:429–441, 1996.
- [25] S. G. Hoggar.  $t$ -designs in projective spaces. *Eur. J. Comb.*, 3:233–254, 1982.

- [26] Y. Hong. On spherical  $t$ -designs in  $\mathbb{R}^2$ . *Eur. J. Comb.*, 3:255–258, 1982.
- [27] J. E. Humphreys. Reflection groups and Coxeter groups. *Cambridge University Press*, 1990.
- [28] R. Kane. Reflection Groups and Invariant Theory. *Springer*, CMS Books in Mathematics, 2001.
- [29] Y. Katznelson. An Introduction to Harmonic Analysis. *Cambridge University Press*, 2004.
- [30] J. Korevaar and J. L. H. Meyers. Spherical Faraday cage for the case of equal point charges and Chebychev-type quadrature on the sphere. *Integral Transforms Spec. Funct.*, 1:105–117, 1993.
- [31] A. Lindblad. Asymptotically optimal  $t$ -design curves on  $\mathbb{S}^3$ . *arXiv:2408.04044*, 2024.
- [32] H. Martini. A hierarchical classification of Euclidean polytopes with regularity properties. In *Polytopes: Abstract, Convex and Computational*, Springer, 71–96, 1994.
- [33] J. Marzo. Marcinkiewicz-Zygmund inequalities and interpolation by spherical harmonics. *J. Funct. Anal.*, 250(2):559–587, 2007.
- [34] J. Marzo and J. Ortega-Cerdà. Equivalent norms for polynomials on the sphere. *Int. Math. Res. Not. IMRN*, (5):Art. ID rnm 154, 18, 2008.
- [35] A. D. McLaren. Optimal numerical integration on a sphere. *Math. Comp.*, 17:361–383, 1963.
- [36] B. Meyer. On the symmetries of spherical harmonics. *Canadian J. Math.*, 6:135–157, 1954.
- [37] H. Nozaki. On the rigidity of spherical  $t$ -designs that are orbits of reflection groups  $E_8$  and  $H_4$ . *Eur. J. Comb.*, 29:1696–1703, 2008.
- [38] M. Reimer. Hyperinterpolation on the sphere at the minimal projection order. *J. Approx. Theory*, 104(2):272–286, 2000.
- [39] B. Reznick. Some constructions of spherical 5-designs. *Linear Algebra Appl.*, 226-228:163–196, 1995.
- [40] J. J. Seidel. Definitions for spherical designs. *J. Statist. Plann. Inference*, 95(1-2):307–313, 2001.
- [41] N. J. A. Sloane, R. H. Hardin, and P. Cara. Spherical designs in four dimensions. *IEEE Information Theory Workshop*, 253–258, 2003.
- [42] S. L. Sobolev. Cubature formulas on a sphere invariant with respect to any finite group of rotations. *Dokl. Akad. Nauk SSSR*, 146(2):310–313, 1962.
- [43] P. Solé. The covering radius of spherical designs. *Eur. J. Comb.*, 12:423–431, 1991.
- [44] E. Stein and G. Weiss. *Introduction to Fourier Analysis on Euclidean Spaces*. Princeton University Press, Princeton, N.J., 1971.
- [45] J. Unnikrishnan and M. Vetterli. Sampling and reconstruction of spatial fields using mobile sensors. *IEEE Trans. Signal Process.*, 61(9):2328–2340, 2013.
- [46] J. Unnikrishnan and M. Vetterli. Sampling high-dimensional bandlimited fields on low-dimensional manifolds. *IEEE Trans. Inform. Theory*, 59(4):2103–2127, 2013.
- [47] Robin J. Wilson. *Introduction to Graph Theory*. Addison Wesley, Longman Limited, 1998.
- [48] M. Winter. Eigenpolytopes, spectral polytopes and edge-transitivity. *arXiv:2009.02179*, 2020.
- [49] M. Winter. Spectral Realizations of Symmetric Graphs, Spectral Polytopes and Edge-Transitivity. *PhD-thesis*, <https://nbn-resolving.org/urn:nbn:de:bsz:ch1-qucosa2-752155>.
- [50] R. Winter and R. van Luijk. The action of the Weyl group on the  $E_8$  root system. *Graphs Combin.*, 37(6):1965–2064, 2021.
- [51] Wolfram Research, Inc., Mathematica, Version 14.1, Champaign, IL (2024).
- [52] R. S. Womersley. Efficient spherical designs with good geometric properties. In J. Dick, F. Kuo, and H. Wozniakowski, editors, *Contemporary Computational Mathematics - A Celebration of the 80th Birthday of Ian Sloan*, Springer, 1243–1285, 2018.

## A Table of some edge-transitive convex polytopes

We list some edge-transitive convex polytopes with their  $t$ -homogeneous symmetry groups in Table 3.

polytope	symmetry	$t$	# vertices	# edges	$\ell(\gamma)$
[rectified] $d$ -tetrahedron	$A_d$	2	$d + 1$	$\binom{d+1}{2}, [(d-1)]$	$\binom{d+1}{2} \arccos(-\frac{1}{d}) \frac{3-(-1)^d}{2}$
[rectified] $d$ -octahedron	$B_d$	3	$2d$	$2(d-1)d [(2d-4)]$	$(d-1)d\pi$
[rectified] $d$ -cube	$B_d$	3	$2^d$	$d2^{d-1} [(d-1)]$	$d \cdot 2^{d-1} \cdot \arccos(\frac{d-2}{d}) \frac{3-(-1)^d}{2}$
[rectified] icosahedron	$H_3$	5	12	30 [60]	$2 \cdot 30 \cdot \arccos(\frac{1}{\sqrt{5}})$
[rectified] dodecahedron	$H_3$	5	20	30 [60]	$2 \cdot 30 \cdot \arccos(\frac{\sqrt{5}}{3})$
[rectified] 24-cell	$F_4$	5	24	96 [288]	$32\pi$
[rectified] 120-cell	$H_4$	11	600	1200 [3600]	$1200 \cdot \arccos(\frac{5+\sqrt{5}}{8})$
[rectified] 600-cell	$H_4$	11	120	720 [3600]	$720 \cdot \arccos(\frac{1+\sqrt{5}}{4})$
cubeoctahedron	$B_3$	3	12	24	$8\pi$
rhomboh dodecahedron	$B_3$	3	14	24	$2 \cdot 24 \cdot \arccos(\frac{1}{\sqrt{3}})$
icosidodecahedron	$H_3$	5	30	60	$12\pi$
rhomboh triacontahedron	$H_3$	5	32	60	$2 \cdot 60 \cdot \arccos(\sqrt{\frac{5+2\sqrt{5}}{15}})$
$4 \leq d$ -demi-cube	$D_d$	3	$2^{d-1}$	$d(d-1)2^{d-3}$	$2 \cdot d(d-1)2^{d-3} \cdot \arccos(\frac{d-4}{d})$
$2_{21}$	$E_6$	4	27	216	$216 \cdot \arccos(\frac{1}{4})$
$3_{21}$	$E_7$	5	56	756	$2 \cdot 756 \cdot \arccos(\frac{1}{3})$
$4_{21}$	$E_8$	7	240	6720	$2240\pi$

TABLE 3. List of some edge-transitive polytopes with  $t$ -homogeneous symmetry groups. The length  $\ell(\gamma)$  of the geodesic cycle  $\gamma$  already contains the factor 2 if edge doubling was required.



## B Proof of Lemma 4.1

We follow the first part of the proof of [16, Theorem 2.2]. According to the definition of the covering radius  $\delta := \delta(\text{supp}(\mu))$ , there is  $x \in \mathbb{S}^d$  such that the closed ball  $B_{\delta/2}(x) = \{y \in \mathbb{S}^d : \text{dist}(x, y) \leq \frac{\delta}{2}\}$  of radius  $\delta/2$  centered at  $x$  does not intersect  $\text{supp}(\mu)$ , i.e.,

$$(9) \quad B_{\delta/2}(x) \cap \text{supp}(\mu) = \emptyset.$$

Let us denote the Laplace-Beltrami operator on the sphere  $\mathbb{S}^d$  by  $\Delta$  and the identity operator by  $I$ . According to [10, Lemma 5.2 with  $s = 2d$  and  $p = 1$ ], see also [8] for the original idea, there is a constants  $c_d > 0$  and a function  $\pi$  supported on  $B_{\delta/2}(x)$  such that

$$(10) \quad \|(I - \Delta)^d \pi\|_{L^1(\mathbb{S}^d)} \leq 1, \quad \text{and} \quad \delta^{2d} \leq c_d \int_{\mathbb{S}^d} \pi.$$

Since (9) implies  $\int_{\mathbb{S}^d} \pi(x) d\mu(x) = 0$ , the exact integration (2) and [8, Theorem 2.12] lead to

$$(11) \quad \left| \int_{\mathbb{S}^d} \pi \right| \leq c'_d t^{-2d} \|(I - \Delta)^d \pi\|_{L^1},$$

for some constant  $c'_d > 0$ . By combining (11) with (10), we deduce

$$\delta^{2d} \leq c_d c'_d t^{-2d} \|(I - \Delta)^d \pi\|_{L^1(\mathbb{S}^d)} \leq c_d c'_d t^{-2d},$$

so that we conclude  $\delta \leq C_d t^{-1}$ , for  $C_d = (c_d c'_d)^{\frac{1}{2d}}$ .